DOI: 10.1002/ejic.201200140

Preparation and Properties of Octadecahedral α-Fe_2O_3 Nanoparticles Enclosed by {104} and {112} Facets

Zhong Liu,[a,b] Baoliang Lv,*[a] Dong Wu,[a] Yuhan Sun,*[a,c] and Yao Xu[a]

Keywords: Solid-state structures / Nanoparticles / Magnetic properties / Sensors

Octadecahedral α-Fe_2O_3 nanoparticles were hydrothermally synthesized in the presence of formamide. These octadecahedral α-Fe_2O_3 nanoparticles have a threefold axis and are enclosed by twelve dominant {112} facets and six {104} facets. In comparison with the {104} facets, the sterically less hindered {112} facets induced the selective adsorption of formamide more easily, which resulted in the gradual increase in the amount of {112} facets by decreasing the amount of {104} facets with increasing formamide. The coercivity (H_c) of these octadecahedral particles increased successively as the aspect ratio (c/a) increased. The sensing capability of these particles toward H_2O_2 was investigated, and the response currents of the particles dominated by {112} facets showed a linear relationship with a concentration of H_2O_2 in the range from 40 μM to 6.66 mM in different stages.

Introduction

The most stable iron oxide under ambient conditions, hematite (α-Fe_2O_3) is used in pigments,[1] catalysts,[2] magnetic recording media,[3] water splitting,[4] anticorrosion agents, and gas sensors[5] owing to its low cost and environmental friendliness. Many efforts were devoted to preparing α-Fe_2O_3 nanocrystals with different geometries and exposed surfaces to explore their shape-dependent properties.[6] For instance, dodecahedral and octadecahedral α-Fe_2O_3 particles showed much stronger magnetism with exposed {101} and {111} facets,[7] and tetradecahedral α-Fe_2O_3 nanoparticles lost ferromagnetism at temperatures lower than the Morin transition temperature (T_m) and exhibited excellent gas-sensing selectivity towards ethanol vapor.[6b,8] In order to prepare nanomaterials with new morphologies, structure evolution of particular morphologies has received increasing attention. For instance, Sun and co-workers described tailoring the process of spindle-particle formation along the [001] direction in the presence of $H_2PO_4^-$, and the particles could be tailored to nanotubes or semitubular structures.[9] In addition, they subsequently prepared α-Fe_2O_3 nanorings by tailoring capsule-shaped α-Fe_2O_3 nanoparticles along the [001] direction.[10] Our group obtained hexagonal nanorings by tailoring hexagonal-bipyramidal particles along the [001] direction in the presence of SCN^-.[11] Notably, all of these morphology-evolution processes were all along the [001] direction and were all obtained with the assistance of inorganic anions. However, the inorganic anions can easily enter the α-Fe_2O_3 lattice and are difficult to remove. In comparison with inorganic anions, organic compounds have less influence on the purity of α-Fe_2O_3 and can be removed easily from the surface by sintering or extraction. As an organic ligand, the adsorption of formamide on different metal or metal oxide surfaces has been reported, such as Ni{111}, Ru{001}, Ag{111}, and TiO_2{011} facets.[12] Based on these results, we speculate that formamide may also adsorb and affect the growth behavior of α-Fe_2O_3 particles with its carbonyl or amino group.

In this work, octadecahedral α-Fe_2O_3 nanocrystals with new exposed facets were synthesized by using a facile hydrothermal method, and dominant facets could change from {104} to {112} successively. Furthermore, the magnetic properties and electrochemical capabilities of these octadecahedral α-Fe_2O_3 nanocrystals were investigated.

Results and Discussion

The purity and crystallinity of the typically synthesized product was determined by XRD (Figure 1a). All peaks in the pattern can be perfectly indexed to hematite (α-Fe_2O_3, JCPDS 33-0664). The morphologies of the product were investigated by scanning electron microscopy (SEM). Figure 1b–d shows typical SEM images at different magnifications. The low-magnification image (Figure 1b) clearly reveals that the products are uniform polyhedra with sizes near 150 nm. As shown in the high-magnification SEM images (Figure 1c and d), the particles are bound by six top

[a] Key Laboratory of Carbon Materials, Institute of Coal Chemistry, Chinese Academy of Sciences, Taiyuan 030001, China
Fax: +86-351-4041153
E-mail: lbl604@sxicc.ac.cn
yhsun@sxicc.ac.cn
[b] Key Laboratory of Salt Lake Resources and Chemistry, Qinghai Institute of Salt Lakes, Chinese Academy of Sciences, Xining 810008, China
[c] Low Carbon Conversion Center, Shanghai Advanced Research Institute, Chinese Academy of Sciences, Shanghai 201203, China

planes and twelve side planes. The cross-section in the middle of these particles is a regular hexagon, and these polyhedral particles have a threefold axis.

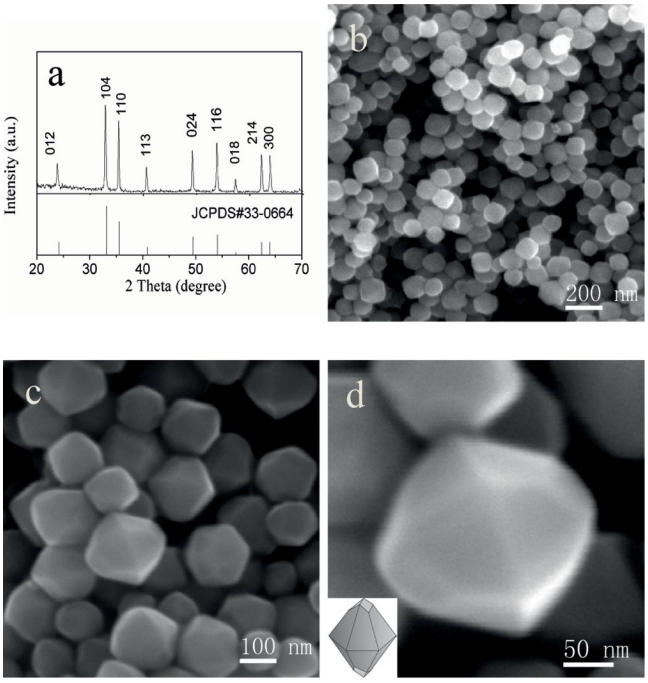

Figure 1. XRD patterns (a) and SEM images (b–d) of typical α-Fe_2O_3 nanoparticles.

To investigate the crystal structure of the polyhedral particles, TEM and high-resolution transmission electron microscopy (HRTEM) analyses were performed. Figure 2a shows the top-view TEM image of a single octadecahedral particle, and Figure 2b shows its corresponding selected area electron diffraction (SAED) pattern. The sharp diffraction spots reveal the single-crystalline nature of the octadecahedral particle, and the diffraction spots can be attributed to the (1–12), (101), and (01–1) planes and/or their equivalent planes under the incident electron beam in the [1–1–1] direction. Figure 2c shows the HRTEM image of the corner of a particle in which three continuous lattice fringes can be resolved, the interplanar distances of which agree well with {1–12}, {101}, and {01–1} facets. This is consistent with the results obtained from the SAED pattern. Figure 2d shows the TEM image of a side view of a single octadecahedral particle, and Figure 2e and f are HRTEM images of regions e and f in Figure 2d, respectively. The inset in Figure 2f shows the corresponding fast Fourier transform (FFT) pattern. From the edge of the particle (Figure 2e), the top facets can be indexed to {–114} or equivalent facets. At the corner of the particle (Figure 2f), two kinds of lattice fringes are identified, the interplanar distances of which are scaled to 0.273 and 0.368 nm, which match the {–114} and {1–12} or equivalent facets, respectively. Based on this evidence and the highly symmetric structure of the particles, it was concluded that the octadecahedral α-Fe_2O_3 was enclosed by six {104} and twelve {112} facets. The six equivalent top planes were indexed to (104), (0–14), (–114), (01–4), (–10–4), and (1–1–4), and the twelve equivalent side planes are (112), (2–12), (1–22), (–1–12), (–212), (–122), (11–2), (2–1–2), (1–2–2), (–1–1–2), (–21–2), and (–12–2). In Figure 2g, a geometrical model of the ideal octadecahedron enclosed by these facets is presented.

According to our previous work, without the addition of formamide, the product consists of quasispherical α-Fe_2O_3 nanoparticles;[13] thus, the presence of formamide should play a crucial role in the morphological evolution of octade-

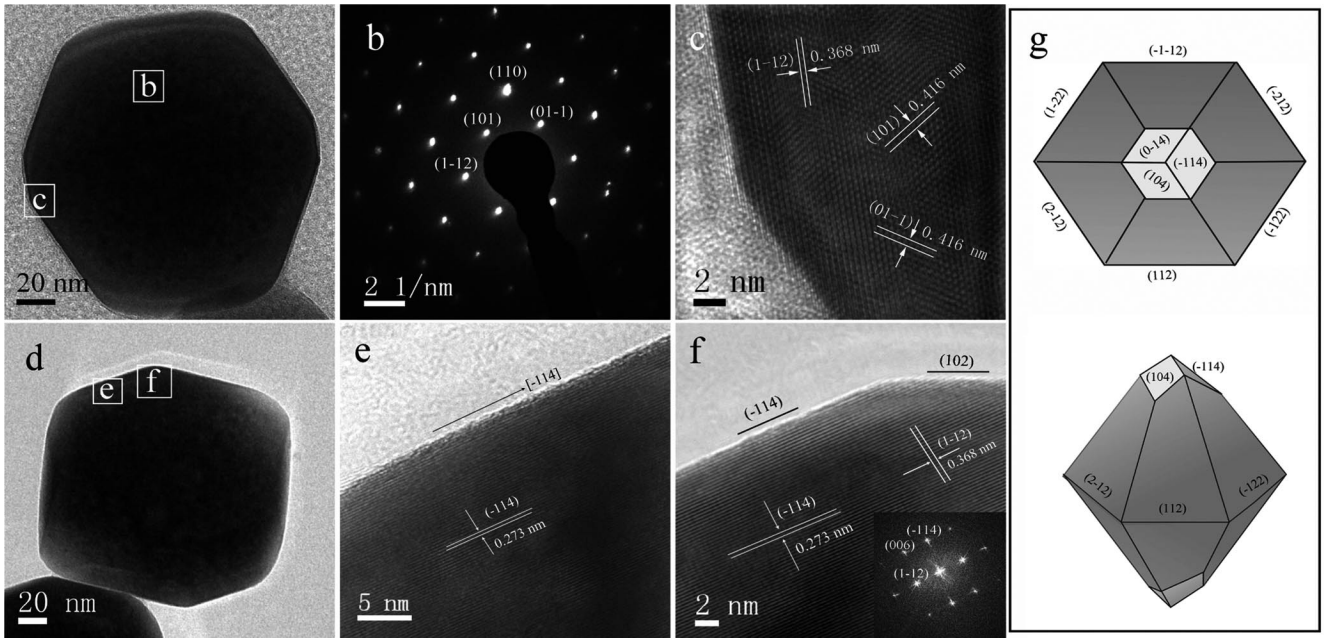

Figure 2. (a) Top-view TEM image of a single octadecahedral α-Fe_2O_3 particle; (b) SAED pattern and (c) HRTEM image of the particle shown in (a); (d) side-view TEM image of a single octadecahedral α-Fe_2O_3 particle; (e) and (f) HRTEM images of different regions in (d), inset in (f) is its corresponding FFT pattern; (g) geometric models of the octadecahedral α-Fe_2O_3 particle.

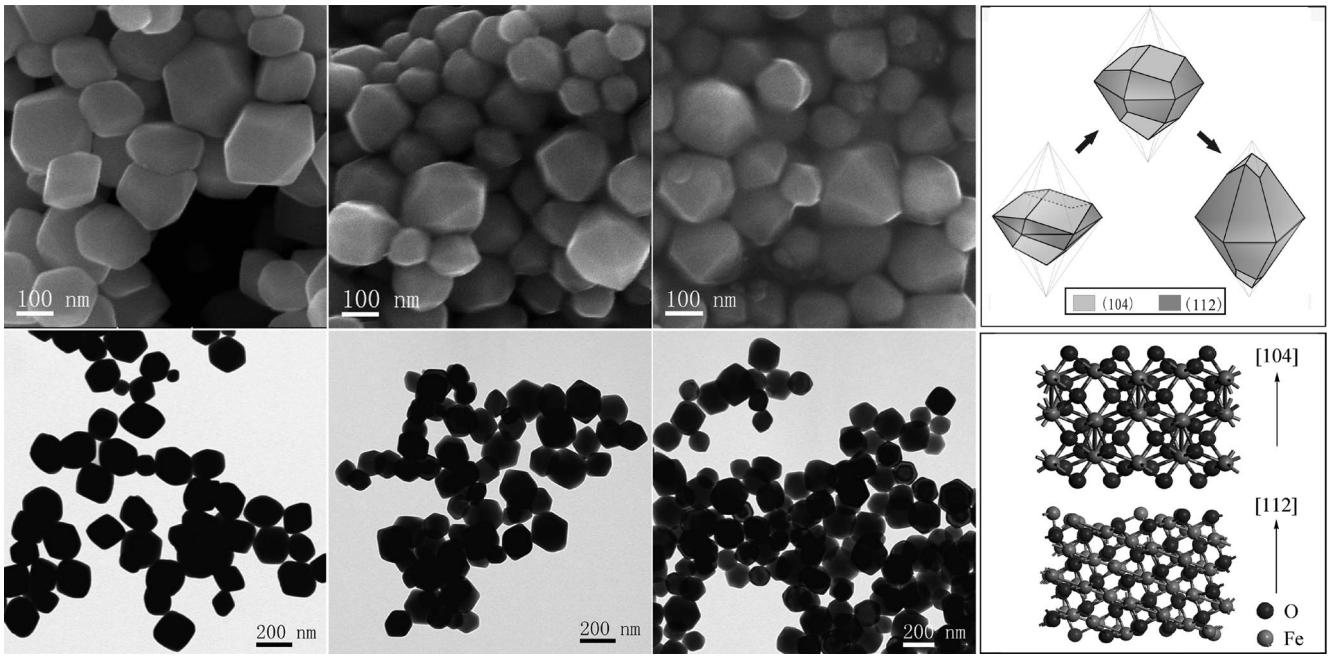

Figure 3. SEM and TEM images of octadecahedral α-Fe_2O_3 particles obtained with the addition of 1.8 (a–b), 5 (c, d), and 12 mL (e, f) of formamide; evolution process of {112} facets (g) and side-view crystal structure of the {104} and {112} facets (h).

cahedral α-Fe_2O_3 nanoparticles. To investigate the detailed effect of formamide, concentration-dependent experiments were carried out. Figure 3 shows SEM and TEM images of α-Fe_2O_3 nanoparticles obtained by adding different amounts of formamide. With an increasing amount of formamide, the dominant facets of octadecahedral α-Fe_2O_3 have a sequential variation from {104} to {112} facets (Figure 3a–f). The morphologies of these particles changed continuously as the aspect ratio (*c*/*a*) increased (Figure 3g), and the size stayed at approximately 150 nm. Figure 3h shows the crystal structure of the {104} and {112} facets, which dominate the particle surfaces. It is speculated that the selective adsorption of formamide causes the number of {112} facets to increase with a decrease in the number of {104} facets. To identify the adsorption of formamide, X-ray photoelectron spectroscopy (XPS) was carried out on typical octadecahedral particles, and the results are shown in Figure 4. The binding energies are corrected for specimen charging by referencing the C 1s line to 284.8 eV, and the spectrum reveals that the octadecahedron surfaces are mainly composed of Fe and O. However, peaks at binding energies of 399.47 eV for N 1s can be observed, which could be attributed to the surface adsorption of formamide.[12d] According to Yang and co-workers,[6b] the selective adsorption of formamide to α-Fe_2O_3 depends on the crystal structures of the facets. As the aforementioned analysis shows, only {104} and {112} facets are exposed on these polyhedral particles. Seen from the crystal structures of the {104} facets (Figure 3h), they are mainly terminated by oxide ions, which can block the adsorption of formamide by steric hindrance. Compared with the {104} facets, some Fe^{3+} ions are exposed on the surface of the {112} facets (Figure 3h), which will facilitate the adsorption of formamide. Generally, there are several possible types of adsorption of formamide on metal or metal oxide surfaces.[12b] To confirm the adsorption type, IR analysis was carried out on the typical octadecahedral particles (Figure 5). The existence of adsorbed formamide can be confirmed easily: the band at 1387 cm^{-1} can be indexed to the deformation of CH, that at 1612 cm^{-1} is an NH_2 stretch, that at 1735 cm^{-1} is the deformation of the carbonyl group, and the peak at 2850 cm^{-1} is a CH stretch.[14] In addition to the NH_2 stretch, the broad absorption at 3050–3550 cm^{-1} may be attributed to a C=O stretch, NH_2 deformation, and hydroxy stretch. The deformation of CH and the carbonyl stretch indicated that the formamide adsorption is of η^1(O)–

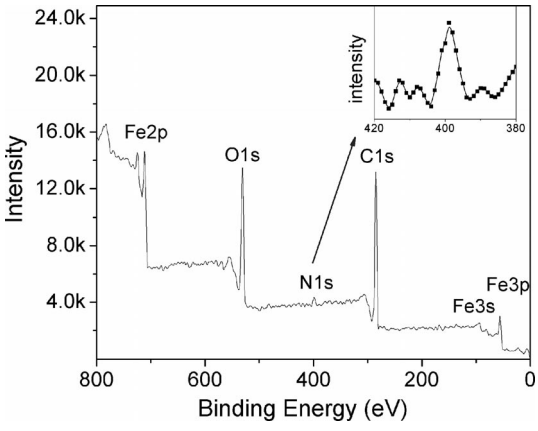

Figure 4. XPS spectrum of the octadecahedral α-Fe_2O_3 particles and high-resolution spectrum of the N 1s region (inset).

$CONH_2$-type.[14] The adsorption is mainly achieved by the Lewis acid–Lewis base interaction between the carbonyl group and Fe^{3+}, and thus restrains the growth process of octadecahedral α-Fe_2O_3 nanoparticles on the {112} facets.[12d] With an increasing amount of formamide, the adsorption on the {112} facets increases accordingly. This would directly result in the slow growth of the {112} facets and thus make the area of {112} facets increase gradually to finally dominate the particle surface.

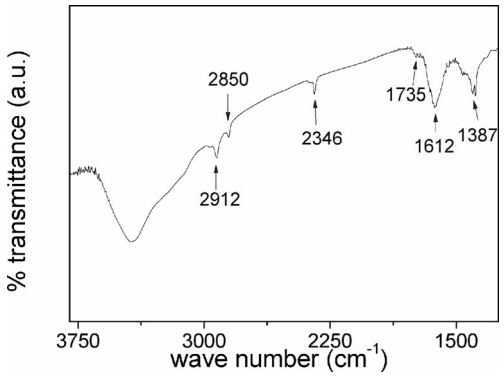

Figure 5. IR spectrum of the octadecahedral α-Fe_2O_3 particles.

The magnetic properties of nanomaterials are considered to be precisely correlated with their size, structure, shape, etc.[6c] α-Fe_2O_3 is an important magnetic material, and it is of great interest to investigate the shape-dependent magnetic properties in the evolution process. Figure 6 shows the room-temperature field-dependent magnetization plots and the table inset shows the values of remnant magnetization (M_r) and coercivity (H_c) of the four α-Fe_2O_3 nanoparticles. Curves a–d in Figure 6 present the hysteresis loops of the four α-Fe_2O_3 nanoparticles obtained by adding 1.8, 5, 10, and 12 mL of formamide, which are shown in Figures 3a, 3c, 1d, and 3e, respectively. Seen from the table inset in Figure 6, the coercivities of these samples increases with the increasing amount of formamide, though the values of curve b are close to those of curve c because of their similar particle size and morphology. In the whole morphological evolution process, the volume of these α-Fe_2O_3 nanoparticles increased with increasing aspect ratio (*c*/*a*), and the successive increase in coercivity with increasing volume is attributed to the increase in magnetic anisotropy, as an applied field at a given temperature should be able to overcome the energy barrier and change the orientation of magnetization.[15]

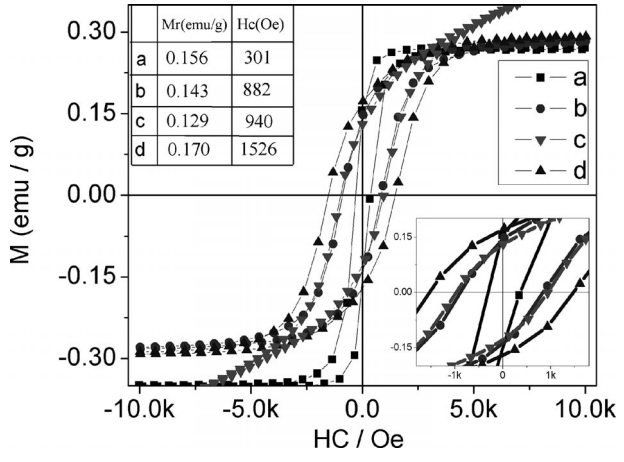

Figure 6. Magnetization loops for α-Fe_2O_3 particles and the values of remnant magnetization and coercivity (inset). The curves (a)–(d) correspond to samples obtained with 1.8, 5, 10, and 12 mL of formamide, respectively.

As the most stable iron oxide, α-Fe_2O_3 is potentially suitable for detecting hydrogen peroxide in a physiological system (pH = 7.2).[16] Because the dominant {112} facets are high-index and high-surface-energy facets,[17] the sensing properties of these α-Fe_2O_3 particles might be enhanced. Figure 7A shows the typical amperometric response of the octadecahedral α-Fe_2O_3-modified glassy carbon (GC) electrode to the successive addition of H_2O_2 at an applied potential of –0.5 V in pH = 7.2 phosphate-buffered saline (PBS) solution, which is the potential of the peak of the

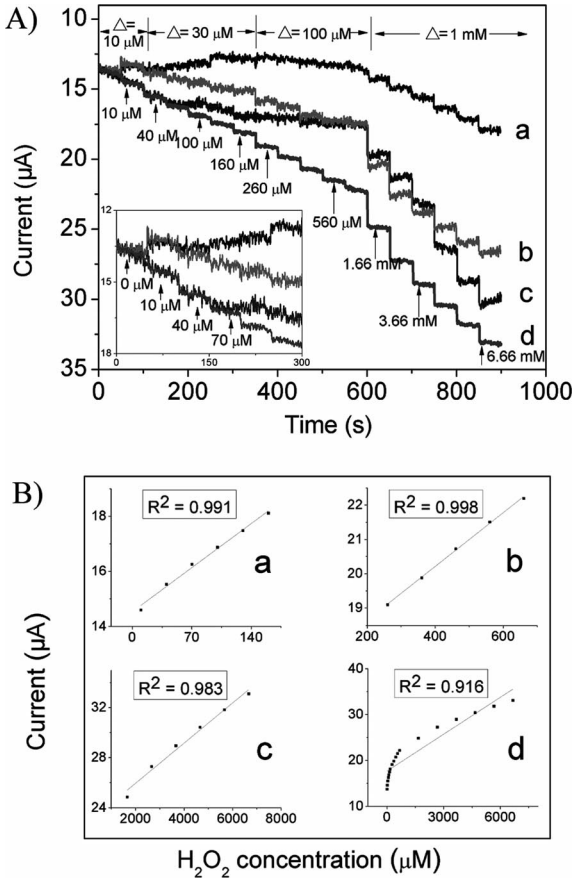

Figure 7. (A) Amperometric response of the octadecahedral α-Fe_2O_3 particles obtained with 1.8 (a), 5 (b), 10 (c), and 12 mL (d) formamide on a GC electrode with successive addition of H_2O_2 from 40 μM to 6.66 mM in PBS (pH = 7.2) at an applied potential of –0.5 V (vs. SCE) (inset: high-resolution plot of first 300 s). (B) Calibration curves of α-Fe_2O_3 particles obtained with 12 mL of formamide with the H_2O_2 concentration at 30 μM (a), 100 μM (b), and 1 mM (c) every time and all concentrations (d), respectively.

H_2O_2 reduction.[16] Curves a–d in Figure 7A present the amperometric response of the four α-Fe_2O_3 nanoparticles obtained by adding 1.8, 5, 10, and 12 mL of formamide, which are shown in Figures 3a, 3c, 1d, and 3e, respectively. When the concentration of H_2O_2 reached 1.66 mM, all the four α-Fe_2O_3 nanoparticles have sensing capability by the regular increase in current. However, only when the particles are dominated by {112} facets (Figure 3e) did the current increase significantly and regularly at an H_2O_2 concentration below 1.66 mM. Figure 7B shows the corresponding calibration curves, which present the sensing capability of {112}-facet-dominated particles at different H_2O_2 concentrations (Figure 3e). When a fixed concentration of H_2O_2 was added in three parts (30 μM, 100 μM, and 1 mM), the current increased as a linear response to the concentration of H_2O_2 (curves a–c in Figure 7B). However, when the concentration of H_2O_2 increased more than 1 mM each time (curve d in Figure 7B), the current obtained experimentally was lower than that predicted by linear theory. This result may be due to the limit of the diffusion speed of H_2O_2 transit to the electrode at high concentration and the limit of the electrode areas. The experimental conditions were similar to those of MnO_2 and prussian blue/multiwalled carbon nanotube hybrid modified electrodes for H_2O_2 detection.[18] The different sensing capability of these four octadecahedral α-Fe_2O_3 nanoparticles may be related to the crystal structure of α-Fe_2O_3. As shown in Figure 3h, the concentration of exposed Fe^{3+} ions on the {112} facets is higher than that on the {104} facets, which may lead to (112) planes possessing better conductivity than (104) planes. In addition, an electron hopping along the [112] direction can cross less O^{2-} ions than that along the [104] direction, and thus the electron can transfer to the surface more quickly when more {112} facets are exposed.[19] Therefore, as the amount of {112} facets increases in the morphological evolution, the octadecahedral α-Fe_2O_3 nanoparticles have less energy to reduce H_2O_2, and the H_2O_2 detection current is closer to the linear value.

Conclusions

Octadecahedral α-Fe_2O_3 nanoparticles with exposed {104} and {112} facets were synthesized in high yields in the presence of formamide. The amount of {112} facets on octadecahedral α-Fe_2O_3 particles increased with a decrease in the amount of {104} facets, and the octadecahedral α-Fe_2O_3 particle dominated by {112} facets exhibited a good sensing capability toward H_2O_2. The volume of these particles increased with increasing aspect ratio (*c*/*a*), which further led to the successive increase in the coercivity values.

Experimental Section

In a typical experiment, $FeCl_3 \cdot 6H_2O$ (3.6 mmol) and formamide (10 mL) were added to distilled water (60 mL) and stirred until totally dissolved. The solution was then transferred into a 100 mL stainless steel autoclave, kept at 220 °C for 24 h, and then cooled naturally. The products were washed with distilled water and absolute ethanol several times and then dried at 60 °C for 4 h. The other experiments were similar, except the amount of formamide was changed to 1.8, 5, and 12 mL.

Powder XRD patterns of the products were acquired with a Philips X'Pert PRO SUPER X-ray diffractometer. The morphologies of the samples were examined by SEM (X-650) and HRTEM (JEOL-2010). XPS was performed with a PHI 5300x multitechnique system with an Mg-K_α X-ray source (Perkin–Elmer Physical Electronics). IR spectra were collected in the frequency range of 1200–3800 cm^{-1} with a Biorad FTS-6000 FTIR spectrometer equipped with an MTEC model 300 photoacoustic (PAS) detector. The magnetic properties of the samples were measured with a superconducting quantum interference device (SQUID, MPMS-XL5). The electrochemical response was measured with an electrochemical workstation (CHI760A, USA) at room temperature. The preparation of the H_2O_2 sensor and measurement methods were similar to those described by Bai and Li.[18a,20]

Acknowledgments

This work was supported by the National Natural Science Foundation of China (No. 21003147), the Natural Science Foundation of Shanxi (2011011007-3), the Distinguished Young Scholar Project of Institute of Coal Chemistry, Chinese Academy of Sciences (2011SJCRC07), and the State Key Laboratory of Coal Conversion (SKLCC) in-house project (No. 2011BWZ005).

[1] J. Wang, W. B. White, J. H. Adair, *J. Am. Ceram. Soc.* **2005**, *88*, 3449–3454.
[2] H. Liu, Y. Wei, Y. Sun, *J. Mol. Catal. A* **2005**, *226*, 135–140.
[3] M. Tadic, V. Kusigerski, D. Markovic, I. Milosevic, V. Spasojevic, *J. Magn. Magn. Mater.* **2009**, *321*, 12–16.
[4] I. Cesar, K. Sivula, A. Kay, R. Zboril, M. Graetzel, *J. Phys. Chem. C* **2009**, *113*, 772–782.
[5] X. L. Fang, C. Chen, M. S. Jin, Q. Kuang, Z. X. Xie, S. Y. Xie, R. B. Huang, L. S. Zheng, *J. Mater. Chem.* **2009**, *19*, 6154–6160.
[6] a) W. Wang, J. Y. Howe, B. H. Gu, *J. Phys. Chem. C* **2008**, *112*, 9203–9208; b) Y. Yang, H. X. Ma, J. Zhuang, X. Wang, *Inorg. Chem.* **2011**, *50*, 10143–10151; c) J. B. Lian, X. C. Duan, J. M. Ma, P. Peng, T. I. Kim, W. J. Zheng, *Acs Nano* **2009**, *3*, 3749–3761.
[7] B. L. Lv, Z. Y. Liu, H. Tian, Y. Xu, D. Wu, Y. H. Sun, *Adv. Funct. Mater.* **2010**, *20*, 3987–3996.
[8] J. Z. Yin, Z. N. Yu, F. Gao, J. J. Wang, H. A. Pang, Q. Y. Lu, *Angew. Chem. Int. Ed.* **2010**, *49*, 6328–6332.
[9] C. J. Jia, L. D. Sun, Z. G. Yan, L. P. You, F. Luo, X. D. Han, Y. C. Pang, Z. Zhang, C. H. Yan, *Angew. Chem.* **2005**, *117*, 4402; *Angew. Chem. Int. Ed.* **2005**, *44*, 4328–4333.
[10] C. J. Jia, L. D. Sun, F. Luo, X. D. Han, L. J. Heyderman, Z. G. Yan, C. H. Yan, K. Zheng, Z. Zhang, M. Takano, N. Hayashi, M. Eltschka, M. Klaui, U. Rudiger, T. Kasama, L. Cervera-Gontard, R. E. Dunin-Borkowski, G. Tzvetkov, J. Raabe, *J. Am. Chem. Soc.* **2008**, *130*, 16968–16977.
[11] B. L. Lv, Y. Xu, D. Wu, Y. H. Sun, *Chem. Commun.* **2011**, *47*, 967–969.
[12] a) Q. Y. Gao, W. Erley, D. Sander, H. Ibach, J. C. Hemminger, *J. Phys. Chem.* **1991**, *95*, 205–211; b) J. E. Parmeter, U. Schwalke, W. H. Weinberg, *J. Am. Chem. Soc.* **1988**, *110*, 53–62; c) W. Reckien, B. Kirchner, F. Janetzko, T. Bredow, *J. Phys. Chem. C* **2009**, *113*, 10541–10547; d) J. M. R. Muir, H. Idriss, *Surf. Sci.* **2009**, *603*, 2986–2990.

[13] B. L. Lv, Y. Xu, D. Wu, Y. H. Sun, *CrystEngComm* **2011**, *13*, 7293–7298.
[14] W. C. Wu, L. F. Liao, C. C. Chuang, J. L. Lin, *J. Catal.* **2000**, *195*, 416–419.
[15] Q. Song, Z. J. Zhang, *J. Am. Chem. Soc.* **2004**, *126*, 6164–6168.
[16] C. Cummings, M. Bonne, K. Edler, M. Helton, A. McKee, F. Marken, *Electrochem. Commun.* **2008**, *10*, 1773–1776.
[17] U. Aschauer, F. Jones, W. Richmond, P. Bowen, A. L. Rohl, G. M. Parkinson, H. Hofman, *J. Cryst. Growth* **2008**, *310*, 688–698.
[18] a) J. J. Xu, Y. H. Bai, H. Zhang, H. Y. Chen, *J. Phys. Chem. C* **2008**, *112*, 18984–18990; b) J. F. Zhai, Y. M. Zhai, D. Wen, S. J. Dong, *Electroanalysis* **2009**, *21*, 2207–2212.
[19] X. J. Zhang, A. X. Gu, G. F. Wang, B. Fang, Q. Y. Yan, J. X. Zhu, T. Sun, J. Ma, H. H. Hng, *CrystEngComm* **2011**, *13*, 188–192.
[20] J. Y. Li, S. L. Xiong, J. Pan, Y. T. Qian, *J. Phys. Chem. C* **2010**, *114*, 9645–9650.

Received: February 11, 2012
Published Online: July 19, 2012

